Curved Trajectory Effect on Charge-Exchange Collision at Ionospheric Temperatures

A. Ieda[1]

[1]Institute for Space-Earth Environmental Research, Nagoya University, Nagoya, Japan

Corresponding author: Akimasa Ieda (ieda@isee.nagoya-u.ac.jp)

Key Points:

- The charge-exchange collision frequency is enhanced by the long-range attractive polarization force at ionospheric temperatures.
- This enhancement has been ignored in the classic regime, partly due to confusion.
- We derive a theoretical form to express this enhancement using the curved particle trajectory effect.

Abstract

Collision between ions and neutral particles is an essential characteristic of Earth's ionosphere. This ion–neutral collision is usually caused by the polarization of neutral particles. This collision can also be caused by charge exchange, if the particle pair is parental, such as atomic oxygen and its ion. The total collision frequency is not the sum of the polarization and charge-exchange components, but is essentially equal to the dominant component. The total is enhanced only around the classic transition temperature, which is near the ionospheric temperature range (typically 200–2000 K). However, the magnitude of this enhancement has differed among previous studies; the maximum enhancement has been reported as 41% and 11% without physical explanation. In the present study, the contribution of the polarization force to the charge-exchange collision is expressed as a simple curved particle trajectory effect. As a result, the maximum enhancement is found to be 22%. It is discussed that the enhancement has been neglected in classic models partly due to confusion with the glancing particle contribution, which adds 10.5% to the polarization component. The enhancement has been neglected presumably also because there has been no functional form to express it. Such an expression is derived in this study.

Plain Language Summary

Solar radiation partially ionizes Earth's neutral atmosphere to form the ionosphere. The ionosphere is a region of plasma at altitudes between 60 and 800 km. The ionosphere co-exists with the neutral atmosphere, and thus ions collide with neutral particles. The corresponding ion–neutral collision frequency is relatively well known at high temperatures, but is less understood at ionospheric temperatures (200–2000 K), because this type of collision has two components that vary with temperature. Near a transition temperature, the classic models underestimate the total collision frequency. We have derived a theoretical form to calculate the collision frequency at ionospheric temperatures that takes into consideration an enhancement near the transition temperature. The revised collision frequency is higher than the classic values by a maximum of 22%.

1 Introduction

Ions collide with neutral particles in Earth's ionosphere. This ion–neutral collision is represented by the collision cross section or frequency as a function of temperature. Accordingly, an accurate model of the cross section is necessary to study the ionosphere.

There are two types of ion–neutral collision (e.g., Banks & Kockarts, 1973). One is electric-polarization collision, which occurs in all ion–neutral pairs because a neutral particle is polarized by an ion. The corresponding cross section is expressed by a classic theoretical functional form of the polarization collision.

The other is charge-exchange collision, which effectively occurs between an ion and its parent atom, such as O^+ and O, because the energy state is the same before and after the electron-transfer collision. The corresponding cross section has been obtained at high temperatures and expressed by a classic theoretical functional form of the charge-exchange collision. This form is appropriate at high temperatures, but its validity has been less clear at ionospheric temperatures, where the values are extrapolated.

For the parental particle pair, the polarization collision dominates at low temperatures (i.e., low kinetic energy), whereas the charge-exchange collision dominates at high temperatures (Figure 1). The total cross section for momentum transfer is not the sum of the polarization and charge-exchange components (Banks & Kockarts, 1973, p. 211). Instead, the total is equal to the dominant component, except for temperatures near a temperature of transition. The transition temperature classically corresponds to the intersection of the polarization and charge-exchange components in Figure 1. Near the classic transition temperature, the total cross section is higher than the dominant component.

However, the magnitude of the enhancement has diverged in previous studies. The total cross section is sometimes calculated as the root-mean-square average of the two classic components (e.g., Bruno et al., 2010; Capitelli et al., 2013; Levin & Wright, 2004; Murphy, 1995). This formulation results in a maximum enhancement of 41%. In contrast, Banks (1966) stated that the enhancement was only approximately 11%; accordingly, the enhancement is not included in classic models (e.g., Banks & Kockarts, 1973; Schunk & Nagy, 2009).

The purpose of this study is to clarify the enhancement in the total cross section and express it using a simple theoretical functional form. We approximate the contribution of the polarization force to the charge-exchange collision as a simple curved particle trajectory effect. As a result, we find that the maximum enhancement is generally 22%.

The physical parameters are defined in Section 2. The classic basics of the ion–neutral collision are summarized in Section 3. The definition of transition temperature is revised in Section 4. The curve effect is numerically calculated in Section 5. We derive an analytical form of the curve effect on the temperature-dependent charge-exchange cross section in Section 6. This analytical form requires a typical charge-exchange cross section for the curve effect. Four types of such typical cross section are derived and evaluated in Section 7. We discuss the reason why the enhancement is ignored in the classic models in Section 8. Appendix A summarizes the computation of our final equations. Appendix B summarizes the computation of an O^+–O

collision model, which is used as an example in the figures of this study. Appendix C summarizes the gamma function, which is used in the detailed derivations provided in Appendices D and E.

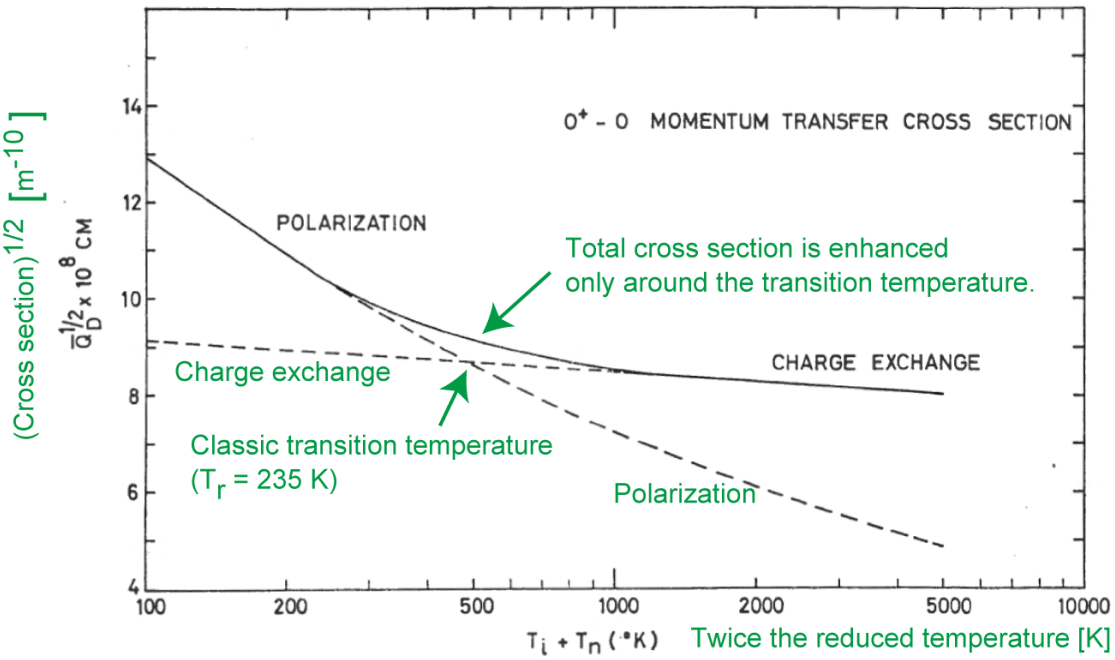

FIG. 2. O^+–O MOMENTUM TRANSFER CROSS SECTION.
The polarization curve is based upon an atomic polarizability of $0{\cdot}89 \times 10^{-24}$ cm³. The charge exchange region is based upon the theoretical work of Knof *et al.*[14] expanded to include the effects of differing ion and neutral gas temperatures.

Figure 1. Figure 2 of Banks (1966) explains the classic model. Reused with permission from Elsevier (license number 5005811313501). Our clarifications are shown in green. The square root of the O^+–O momentum-transfer cross sections are shown against twice the ion–neutral reduced temperature. The solid line shows the total cross section, which consists of two components, shown by the dashed lines. The total is not the sum of the two components, but is essentially equal to the polarization component at low temperatures and to the charge-exchange component at high temperatures. The total cross section is larger than that of either component only around the transition temperature, where the two components intersect. The corresponding maximum enhancement was stated to be 11% in Banks (1966), although it was not explained how the total cross section was calculated.

2 Definitions

The physical parameters used in this study are defined in Table 1. Note that the charge-exchange collision includes both the charge-exchange cross section (CXCS) and the momentum-transfer cross section (MTCS); in contrast, the polarization collision includes only the MTCS.

For the charge-exchange collision, the labels str (straight) and cv (curved) are used when necessary for clarification. The label total refers to the combination of the polarization and charge-exchange components.

111 **Table 1**. *Definitions of Physical Parameters for Ion–Neutral Collision*

Physical parameter	Definition
ε_0	Vacuum electric permittivity, 8.854188×10^{-12} F/m
e	Fundamental charge, $1.602176634 \times 10^{-19}$ C
k_B	Boltzmann constant, 1.380649×10^{-23} J/K
m_u	Unified atomic mass constant, 1.660539×10^{-27} kg
A_r (u)	Relative atomic mass, 16.0 for oxygen atom
m_i, m_n (kg)	Mass (ion, neutral particle)
μ_r (kg)	Reduced mass $m_i m_n/(m_i+m_n)$
α_V (m^3)	Polarizability volume
w_r (J)	Reduced energy[a] $\mu_r g^2/2$
ε_r (eV)	Reduced energy[a] w_r/e
x	Normalized energy $w_r/k_B T_r = e\varepsilon_r/k_B T_r$
T_i, T_n (K)	Temperature (ion, neutral gas)
T_r (K)	Reduced temperature $(m_n T_i+m_i T_n)/(m_i+m_n)$
$Q_{CX}(\varepsilon_r)$ (m^2)	Energy-dependent charge-exchange cross section (CXCS)
$Q_{MT}(\varepsilon_r)$ (m^2)	Energy-dependent momentum-transfer cross section (MTCS)
$S_{CX}(T_r)$ (m^2)	Temperature-dependent CXCS
$S_{MT}(T_r)$ (m^2)	Temperature-dependent MTCS[b]
n_n ($1/m^3$)	Number density of neutral gas
ν_{in} (1/s)	Ion–neutral collision frequency[c]

112 *Note.* The SI unit system is used.

113 [a]This energy is the conventional kinetic energy used in theoretical atomic collision studies, also
114 known as the kinetic energy of the reduced mass particle. See further explanations in Appendix
115 A of Ieda (2021). [b]This is also known as the average diffusion or momentum-transfer cross
116 section $\bar{Q}_D$ in Banks (1966) and Banks and Kockarts (1973), which is the same as the collision
117 integral $\Omega_{1,1}(T)$ in Pesnell et al. (1993) and Hickman et al. (1997a). Note that the term collision
118 integral refers to slightly different quantities in some previous studies (e.g., Schunk & Nagy,
119 2009; Stallcop et al., 1991). [c]"Ion–neutral collision frequency" in this study refers to the collision
120 frequency for momentum transfer from neutral gas to ions in the laboratory frame.

121 ## 3 Classic Basics of Ion–Neutral Collision

122 In this section, we summarize the classic basic concepts associated with collisions between ions
123 and neutral particles. The Langevin cross section is the core part of the polarization cross section.

124 ### 3.1 Collision Cross Section and Frequency

125 The energy-dependent MTCS $Q_{MT}(\varepsilon_r)$ is obtained from theoretical or laboratory studies. $Q_{MT}(\varepsilon_r)$
126 is integrated or weighted-averaged over energy for each temperature to obtain the average or
127 temperature-dependent MTCS $S_{MT}(T_r)$ as follows:

$$S_{\mathrm{MT}}\left(T_{\mathrm{r}}\right)=\frac{1}{2}\int_0^\infty Q_{\mathrm{MT}}x^2\exp\left(-x\right)dx\,, \tag{3-1}$$

where x is the normalized energy defined by

$$x\equiv\frac{w_{\mathrm{r}}}{k_{\mathrm{B}}T_{\mathrm{r}}}=\frac{e\varepsilon_{\mathrm{r}}}{k_{\mathrm{B}}T_{\mathrm{r}}}\,. \tag{3-2}$$

See Table 1 for the definitions of the physical parameters. Equation 3-1 is equivalent to Equation 3 of Dalgarno et al. (1958) and implies an average of $Q_{\mathrm{MT}}(\varepsilon_{\mathrm{r}})$, weighted by a Maxwellian velocity distribution of particles.

$S_{\mathrm{MT}}(T_{\mathrm{r}})$ is associated with the diffusion or momentum-transfer collision frequency ν_{in}, according to

$$\nu_{\mathrm{in}}/n_{\mathrm{n}}=\frac{m_{\mathrm{n}}}{m_{\mathrm{i}}+m_{\mathrm{n}}}\frac{4}{3}\sqrt{\frac{8k_{\mathrm{B}}}{\pi\mu_{\mathrm{r}}}}\sqrt{T_{\mathrm{r}}}S_{\mathrm{MT}} \tag{3-3}$$

in the laboratory frame. This equation is equivalent to Equation 9.78 of Banks and Kockarts (1973).

The collision frequency in Equation 3-3 is widely used in ionospheric studies. For example, it is used to calculate the electric conductivity (e.g., Equation 1 of Ieda et al., 2014). It is also used to express the frictional force or momentum transfer caused by the neutral gas in an ion-fluid equation of motion or momentum equation

$$n_{\mathrm{i}}m_{\mathrm{i}}\frac{d\mathbf{U}_{\mathrm{i}}}{dt}=-\nabla\left(k_{\mathrm{B}}n_{\mathrm{i}}T_{\mathrm{i}}\right)-\nu_{\mathrm{in}}n_{\mathrm{i}}m_{\mathrm{i}}\left(\mathbf{U}_{\mathrm{i}}-\mathbf{U}_{\mathrm{n}}\right), \tag{3-4}$$

where $\mathbf{U}_{\mathrm{i}}$ and $\mathbf{U}_{\mathrm{n}}$ are the fluid velocities of the ion and neutral gases, respectively, and n_{i} is the ion number density.

3.2 Electric Polarizability and Polarizability Volume

When an ion approaches a neutral particle, the ion-associated electric field induces an electric dipole in the neutral particle (Figure 2a). The strength of the induced dipole is proportional to the applied electric field. The corresponding constant factor is called the electric dipole polarizability, and depends on the species of neutral particle.

Previous studies have used the CGS unit system, in which the polarizability α is given in units of α (cm^3) (e.g., Table 1 of Banks, 1966). We use the SI unit system, in which the unit of polarizability is α ($\mathrm{C\,m^2\,V^{-1}}$). Because this unit is not convenient, we use the polarizability volume α_{V} (m^3) instead. These are associated in the SI unit system (e.g., Atkins et al., 2018, p. 710) according to

$$\alpha\left(\mathrm{C^2m^2V^{-1}}\right)=4\pi\varepsilon_0\times\alpha_{\mathrm{V}}\left(\mathrm{m}^3\right). \tag{3-5}$$

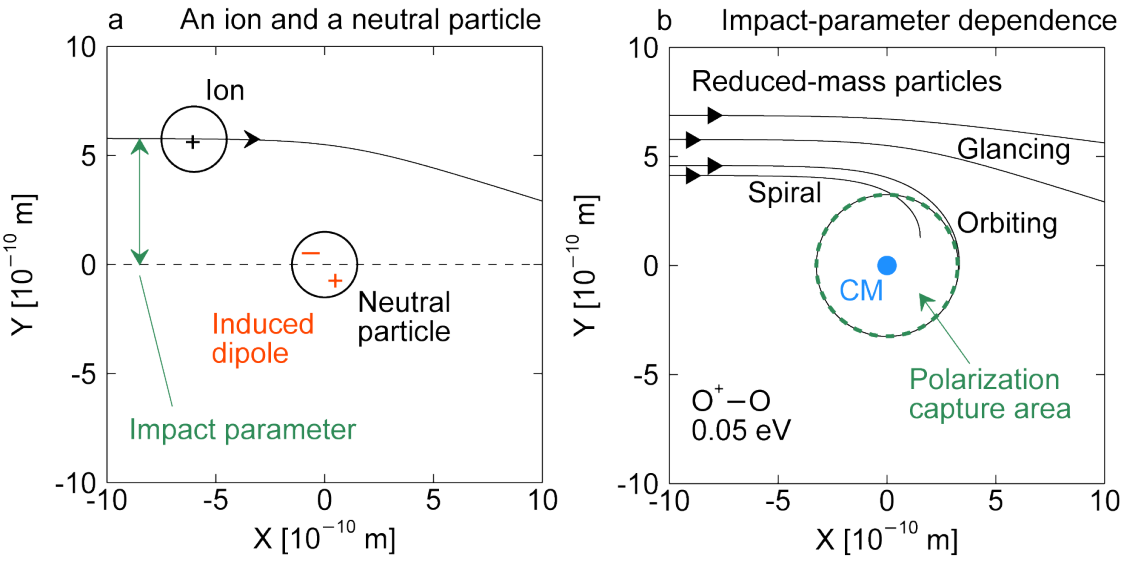

Figure 2. Illustration of the polarization collision between an ion and a neutral particle. (a) The collision in the neutral-particle rest frame for an impact parameter, which corresponds to the Y distance of the ion at $X = -\infty$. The ion induces an electric dipole in the neutral particle. (b) The collision in the center-of-mass (CM) frame for four impact parameters. The ion takes three different types of trajectory as labelled, depending on the impact parameter. The O^+–O collision calculated at a reduced energy of 0.05 eV is shown as an example.

3.3 Particle Orbiting and Langevin Cross Section

The ion and the induced dipole attract each other, meaning that the ion collides with the neutral particle. The two-body problem can be reduced to a one-body problem (McDaniel, 1989, p. 83) with the virtual reduced mass particle interacting with the electric potential of the system, as shown in Figure 2b. The kinetic energy of the reduced mass particle is defined as the reduced energy in Table 1. For each kinetic energy, the significance of the collision depends on the impact parameter.

For the distant collision labeled glancing in Figure 2b, the particle takes a glancing trajectory, where the attractive force is weaker than the centrifugal force. For the close collision labeled spiral in Figure 2b, the particle is captured by the polarization attractive force and then takes a spiral trajectory toward the barycenter. The particle is subsequently reflected by a repulsive core. This reflection is not illustrated in Figure 2b for simplicity.

The two regions of glancing and spiral trajectories are separated by the orbiting trajectory, where the attractive force and the centrifugal force balance at the closest approach. A particle on this orbiting trajectory subsequently undergoes infinite rotation with the orbiting radius R_{orb}. We call the area inside this radius the capture area Q_{cap}, which is given by

$$Q_{\text{cap}} \equiv \pi R_{\text{orb}}{}^2 . \tag{3-6}$$

The spiral motion inside this capture area implies that the particle velocity direction is practically random. Thus, the momentum of the particle is zero on average, and the capture area therefore corresponds numerically to an MTCS.

In addition, the particle trajectory is already curved by the attractive polarization force before entering the capture area. That is, the particle comes from a wider area, and the MTCS is effectively enhanced. This effective energy-dependent MTCS is twice the capture area and is called the Langevin cross section, which is given by

$$Q_{\mathrm{Lan}} = 2Q_{\mathrm{cap}} = e\sqrt{\frac{\pi}{2\varepsilon_0}\frac{\alpha_{\mathrm{V}}}{w_{\mathrm{r}}}} \equiv \sqrt{\frac{C_{\mathrm{Lan}}}{w_{\mathrm{r}}}}\,, \tag{3-7}$$

where the constant C_{Lan} is defined by this equation, which is equivalent to Equation 3-6-6 of McDaniel (1989).

Equation 3-7 is integrated over energy for each temperature to obtain the corresponding temperature-dependent MTCS

$$S_{\mathrm{Lan}} = \frac{1}{2}\frac{3\sqrt{\pi}}{4}\sqrt{\frac{C_{\mathrm{Lan}}}{k_{\mathrm{B}}T_{\mathrm{r}}}} = \frac{3\sqrt{\pi}}{8}\sqrt{\frac{C_{\mathrm{Lan}}}{k_{\mathrm{B}}T_{\mathrm{r}}}}\,. \tag{3-8}$$

3.4 Polarization Collision Cross Section

The glancing particle in Figure 2b is not included in Equation 3-7. It adds 10.5% of the Langevin cross section (Dalgarno et al., 1958; Heiche & Mason, 1970; Kihara et al., 1960; Langevin, 1905). Accordingly, the energy-dependent polarization MTCS is

$$Q_{\mathrm{pol}} = 1.105 \times Q_{\mathrm{Lan}}\,, \tag{3-9}$$

which is equivalent to Equation 4 of Banks (1966). This collision is called the nonresonant collision by Schunk and Nagy (2009); we refer to it as the polarization collision to emphasize the physical mechanism.

The corresponding temperature-dependent MTCS of the polarization collision is obtained by integrating Equation 3-9 over energy for each temperature, or simply by

$$S_{\mathrm{pol}} = 1.105 \times S_{\mathrm{Lan}}\,. \tag{3-10}$$

This equation is equivalent to Equation 5 of Banks (1966).

3.5 Classic Charge-Exchange Cross Section

Charge exchange occurs with a probability of approximately ½ in a reaction area (Figure 3):

$$Q_{\mathrm{CX}}\left(\varepsilon_{\mathrm{r}}\right) = Q_{\mathrm{react}}\left(\varepsilon_{\mathrm{r}}\right)/2\,. \tag{3-11}$$

The polarization force is negligible at high energies in the charge-exchange collision. That is, the particle trajectory is practically straight at high energies. The classic model implicitly assumes a straight trajectory or high energies. Under this condition, the CXCS $Q_{\mathrm{CX}}(\varepsilon_{\mathrm{r}})$ can be approximately given in the form of

$$Q_{\mathrm{CX}}\left(\varepsilon_{\mathrm{r}}\right) = \left(A_0 - B_0 \log_{10}\varepsilon_{\mathrm{r}}\right)^2\,, \tag{3-12}$$

where A_0 and B_0 are constants that depend on the particle species. These constants are obtained from theoretical calculations or laboratory experiments. The ratio A_0/B_0 is relatively constant and is typically between 8 and 10 among the particle pairs that are relevant to ionospheric studies in Banks (1966). This form was theoretically established by Dalgarno (1958). We call this type of CXCS classic or straight, in contrast to effective or curved, which will be explained in the next section.

When $Q_{CX}(\varepsilon_r)$ is given in the form of Equation 3-12, the general integration in Equation 3-1 can be approximated as a semi-analytical integration as

$$S_{CX}^{str}(T_r) \sim \left[A_0 + B_0\left(3.668 - \log_{10} T_r\right)\right]^2 \approx \left[A_0 - B_0 \log_{10}\left(2.492 \times T_r k_B / e\right)\right]^2 \quad (3\text{-}13)$$

(Mason & Vanderslice, 1959; Banks, 1966; Pesnell et al., 1994; Ieda, 2020). See details in Appendix D. Note that the straight particle trajectory also implies the following approximation:

$$\begin{cases} Q_{MT}^{str} = 2 \times Q_{CX}^{str} \\ S_{MT}^{str} = 2 \times S_{CX}^{str} \end{cases}. \quad (3\text{-}14)$$

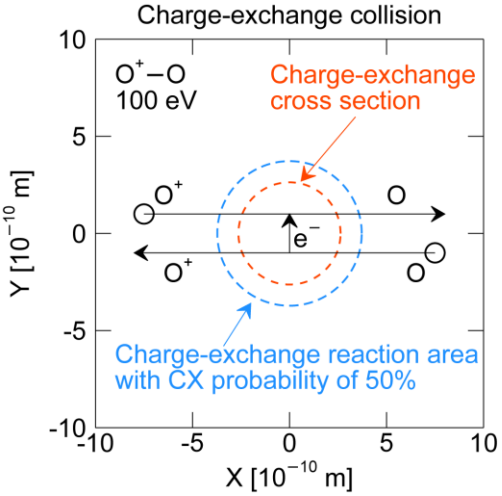

Figure 3. Illustration of the charge-exchange collision with the classic or straight-trajectory assumption. The O^+–O model presented in Appendix B is used at a reduced energy of 100 eV as an example. The charge-exchange collision is caused by an electron transfer to an ion from a parent neutral particle. A simplified average view of this process is shown. In reality, the electron goes back and forth between an ion and a neutral particle. In other words, the probability of an electron transfer is approximately 50% inside the reaction area. Accordingly, the charge-exchange cross section is half the reaction area.

4 Revising the Definition of Transition Temperature

The ion–neutral collision MTCS of the parental particle pair is expressed by different equations between the polarization and charge-exchange domains. The two domains are separated by the transition energy or temperature, which are different between the classic and our regimes, as summarized in Table 2.

Table 2. *Definitions of Transition Energy and Temperature*

Symbol	Type	Defining equation	Value[a] for O^+–O
		Transition energy	
ε_{tran}^{cla} (eV)	Classic	$Q_{MT}^{str} = Q_{pol}$	0.0281 eV
ε_{tran}^{phy} (eV)	Physical	$Q_{MT}^{str} = \frac{Q_{Lan}}{2} \approx \frac{Q_{pol}}{2.21}$	0.00429 eV
		Transition temperature	
T_{tran}^{cla} (K)	Classic	$S_{MT}^{str} = S_{pol}$	147[b] K
T_{tran}^{phy} (K)	Physical	$S_{MT}^{str} = \frac{S_{Lan}}{2} \approx \frac{S_{pol}}{2.21}$	22 K

Note. Classic type separates the polarization and charge-exchange domains in the classic regime (Banks, 1966; Banks & Kockarts, 1973; Schunk & Nagy, 2009), whereas the physical type separates the two domains in the curved regime introduced in this study.

[a]Values are examples specific to the O^+–O collision model defined in Appendix B. [b]Strictly speaking, the classic transition temperature (147 K) in this table is a classic-type transition temperature and is different from the classic transition temperature of 235 K in classic models. These values are different because the basis models are different.

4.1 Definition of Classic Transition Energy and Temperature

Although we cannot find an explicit definition of the classic transition temperature in previous studies, it is presumably defined as the temperature of the intersection in Figure 1, where MTCS is the same for the polarization (Equation 3-10) and classic charge-exchange (Equation 3-14) components. This interpretation is numerically consistent with the transition temperature of Banks (1966). Accordingly,

$$S_{\mathrm{MT}}^{\mathrm{str}} = S_{\mathrm{pol}} = \frac{2.21}{2} S_{\mathrm{Lan}} . \tag{4-1}$$

The corresponding classic transition energy is not defined in most previous studies, but in Heiche and Mason (1970), using

$$Q_{\mathrm{MT}}^{\mathrm{str}} = Q_{\mathrm{pol}}, \tag{4-2}$$

which is analogous to Equation 4-1.

4.2 Definition of Revised Transition Energy and Temperature

As detailed in Section 4.3, a physical transition does not occur at the classic transition energy but at an energy at which the capture and charge-exchange reaction areas are the same:

$$Q_{\mathrm{Lan}} / 2 = Q_{\mathrm{cap}} = Q_{\mathrm{react}} = Q_{\mathrm{CX}}^{\mathrm{str}} \times 2 = Q_{\mathrm{MT}}^{\mathrm{str}} . \tag{4-3}$$

Accordingly, we define a "physical" transition energy using

$$Q_{\mathrm{MT}}^{\mathrm{str}} = \frac{Q_{\mathrm{Lan}}}{2} \approx \frac{Q_{\mathrm{pol}}}{2.21} . \tag{4-4}$$

This physical transition energy is much lower than the classic transition energy.

The corresponding temperature of physical transition is less strict because the temperature-dependent cross section is a weighted average of the energy-dependent cross section. However, it is useful to define a corresponding physical transition temperature as a measure. We define it as

$$S_{\mathrm{MT}}^{\mathrm{str}} = \frac{S_{\mathrm{Lan}}}{2} \tag{4-5}$$

for simplicity in analogy to the physical transition energy in Equation 4-4. This definition is numerically reasonable, as discussed in Section 8.1.

4.3 Physical Implications of the Transition Energies

In the classic regime, the particle trajectory is assumed to be straight in the charge-exchange collision, as described in Section 3.5. The classic transition energy separates the polarization and straight-trajectory charge-exchange domains. In reality, the particle trajectory is curved toward

the charge-exchange reaction area. This curve is not negligible around the transition energy by definition. Thus, the classic transition energy in Equation 4-2 is irrelevant to actual physical transitions but is an artifact or approximation; instead, it is the physical transition energy defined in Equation 4-3 that actually separates the two domains (i.e., the polarization and curved-trajectory charge-exchange domains), as follows.

Figure 4a shows the parental collision below $\varepsilon_{\text{tran}}^{\text{phy}}$, that is, in the polarization or capture domain where $Q_{\text{cap}} > Q_{\text{react}}$. In other words, a small charge-exchange reaction sphere is added to Figure 2b. Under this condition, the captured particles take the spiral trajectory, and their direction is already practically random before the charge-exchange collision. That is, the charge-exchange collision process does not contribute to the momentum transfer. Accordingly, the MTCS is the same as the polarization MTCS in Equation 3-10.

For clarification, in the revised polarization domain, the effective rate of reaction is generally determined by the capture (Gioumousis & Stevenson, 1958). Accordingly, the effective CXCS is

$$Q_{\text{CX}} = Q_{\text{Lan}} / 2 , \tag{4-6}$$

which is consistent with Equation 65 of Rapp and Francis (1962) and is significantly larger than the classic CXCS. That is, the low-energy part of the classic CXCS in Figure 1 merely implies the imaginary charge-exchange component.

In contrast, Figure 4b shows the parental collision above $\varepsilon_{\text{tran}}^{\text{phy}}$, that is, in the charge-exchange domain where $Q_{\text{cap}} < Q_{\text{react}}$. In other words, a large charge-exchange reaction sphere is added to Figure 2b. Under this condition, the particles enter the charge-exchange reaction area before reaching the capture area. Accordingly, the MTCS is basically expressed by Equation 3-14. In addition, this MTCS is effectively enhanced as discussed in the next section.

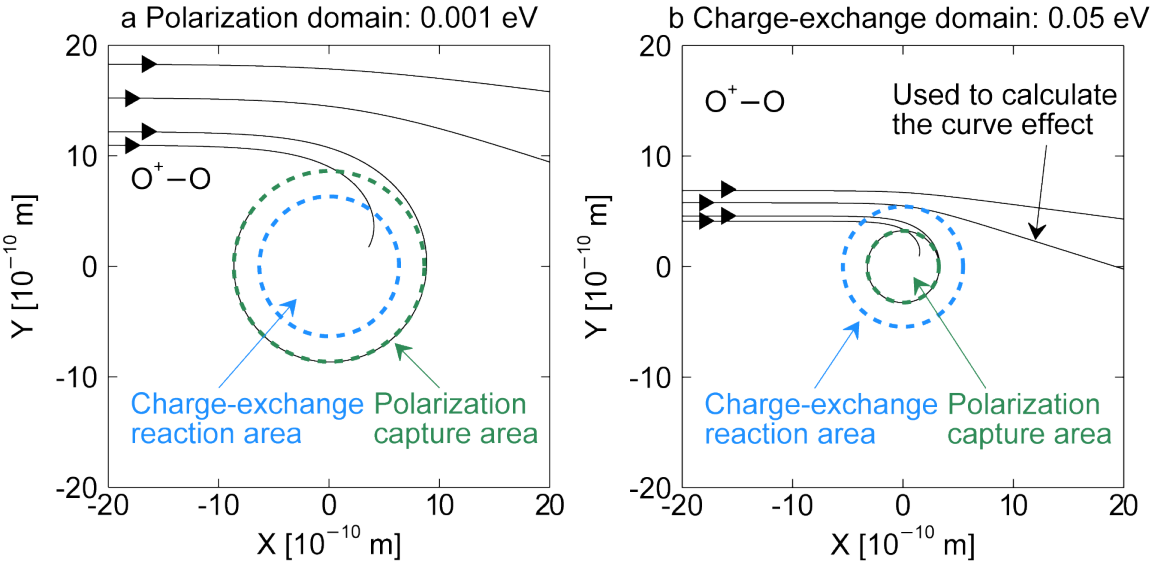

Figure 4. Combination of the polarization and charge-exchange collisions. The charge-exchange reaction area is added to the illustration of the polarization collision shown in Figure 2b. Collision between an ion and a parent neutral particle is represented by a corresponding reduced

mass particle. The O^+–O cross section model presented in Appendix B1 is used as an example. The origin corresponds to the barycenter. The particle takes different types of trajectory depending on the impact parameter, which corresponds to the *Y* distance at $X = -\infty$. (a) Collision at a reduced energy of 0.001 eV in the polarization domain. Charge exchange is irrelevant to the momentum-transfer cross section (MTCS). (b) Collision at 0.05 eV in the charge-exchange domain. The charge-exchange process basically determines the MTCS, which is effectively enhanced in addition by the curved particle trajectories caused by the polarization force.

5 Curved Particle Trajectory Effect

5.1 Curve Effect on Energy-Dependent Cross Section

In the charge-exchange domain, the MTCS is effectively enhanced owing to the curved trajectory outside the charge-exchange reaction area. We call this additional contribution the curved particle trajectory effect.

The curve effect on the energy-dependent CXCS can be derived from the condition that the distance of the closest approach is the same as the radius of the charge-exchange reaction area, as shown in Figure 4b. The resultant effective or curved CXCS $Q_{\mathrm{CX}}^{\mathrm{cv}}(\varepsilon_{\mathrm{r}})$ is

$$Q_{\mathrm{CX}}^{\mathrm{cv}} = Q_{\mathrm{CX}}^{\mathrm{str}}\left[1+\frac{1}{16}\left(\frac{Q_{\mathrm{Lan}}}{Q_{\mathrm{CX}}^{\mathrm{str}}}\right)^2\right], \tag{5-1}$$

where $Q_{\mathrm{CX}}^{\mathrm{str}}(\varepsilon_{\mathrm{r}})$ refers to the classic or straight CXCS, as shown in Equation 3-12. Equation 5-1 is equivalent to Equation 16 of Holstein (1952) and Equation 12 of Wolf and Turner (1968).

Using Equation 3-14 (i.e., $Q_{\mathrm{MT}} = 2Q_{\mathrm{CX}}$), the corresponding MTCS is

$$Q_{\mathrm{MT}}^{\mathrm{cv}} = Q_{\mathrm{MT}}^{\mathrm{str}}\left[1+\frac{1}{4}\left(\frac{Q_{\mathrm{Lan}}}{Q_{\mathrm{MT}}^{\mathrm{str}}}\right)^2\right]. \tag{5-2}$$

Note that Equation 3-14 does not necessarily hold, but is a good approximation at energies above approximately the classic transition energy (Heiche & Mason, 1970). That is, the MTCS in Equation 5-2 is not strictly equal to the actual total MTCS but implies a measure or a component below the classic transition energy.

5.2 Maximum Enhancement in Energy-Dependent Cross Section

Figure 5 shows various components of the energy-dependent MTCS. Most components are explained in Section 3, except for the red line labeled curved CX, which represents the charge-exchange component with the curved trajectory effect in Equation 5-2.

The polarization component intersects with the classic charge-exchange component at 0.0281 eV. Around this classic transition energy, the curved CX component is practically equal to the total cross section. The increase in the total cross section from the greater of the polarization or classic charge-exchange components is called an enhancement. The maximum enhancement is 20.47%, as shown in Figure 5b. Similarly, the maximum enhancement is 25% when the Langevin component is referenced, instead of the polarization component. This 25% can be readily expected from Equation 5-2 and is independent of the particle pair.

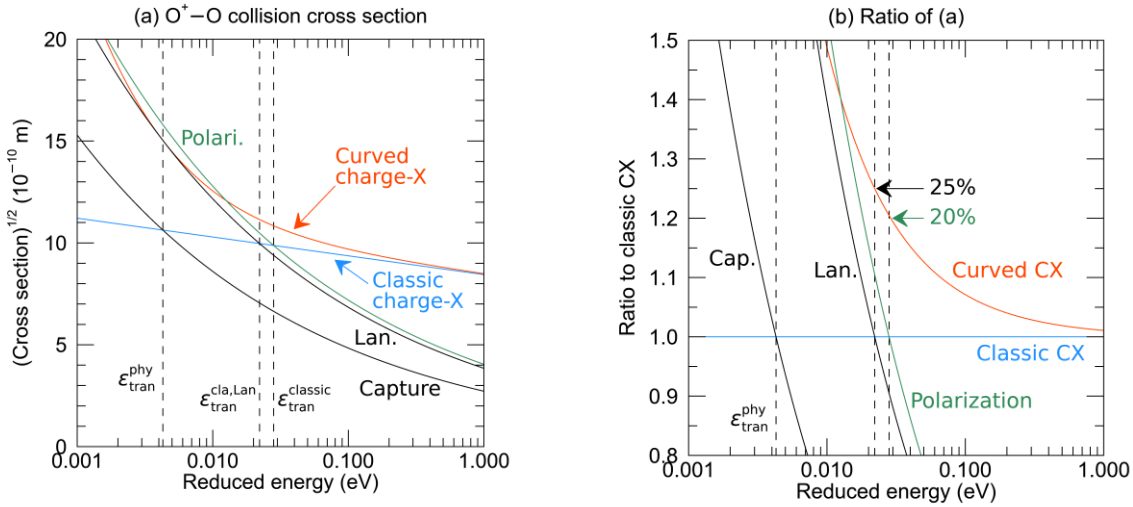

Figure 5. Components of energy-dependent momentum-transfer collision cross sections. The O^+–O cross section model presented in Appendix B1 is used as an example. The charge-exchange (CX) components refer to the charge-exchange cross section multiplied by two. The components include polarization, Langevin, capture, classic CX, and curved or effective CX. The dashed lines indicate transition energies. (a) Square-root of the momentum-transfer cross section. (b) Ratio of the components to the classic CX component. The curved or effective CX component is higher than the greater of the polarization or classic CX components by a maximum of 20.47%.

5.3 Maximum Enhancement in Temperature-Dependent Cross Section

The effective energy-dependent CXCS in Equation 5-2 can be numerically integrated using Equation 3-1. Figure 6 shows the results as the red line labeled curved CX.

We define the enhancement of the total cross section as in the previous section. The maximum enhancement is 22.3% at the classic-type transition temperature of 146.8 K when the polarization component is referenced. This classic-type transition temperature (146.8 K) is somewhat lower than the classic transition temperature (235 K in the classic model) because the basis models are different. The maximum enhancement is 27.3% at 115.7 K when the Langevin cross section is referenced.

For clarification, the transition temperature depends on the particle pair. For example, the classic transition temperature is approximately 600 K for the O_2^+-O_2 collision (Ieda, 2020) and is approximately 50 K for the H^+-H collision (Banks, 1966).

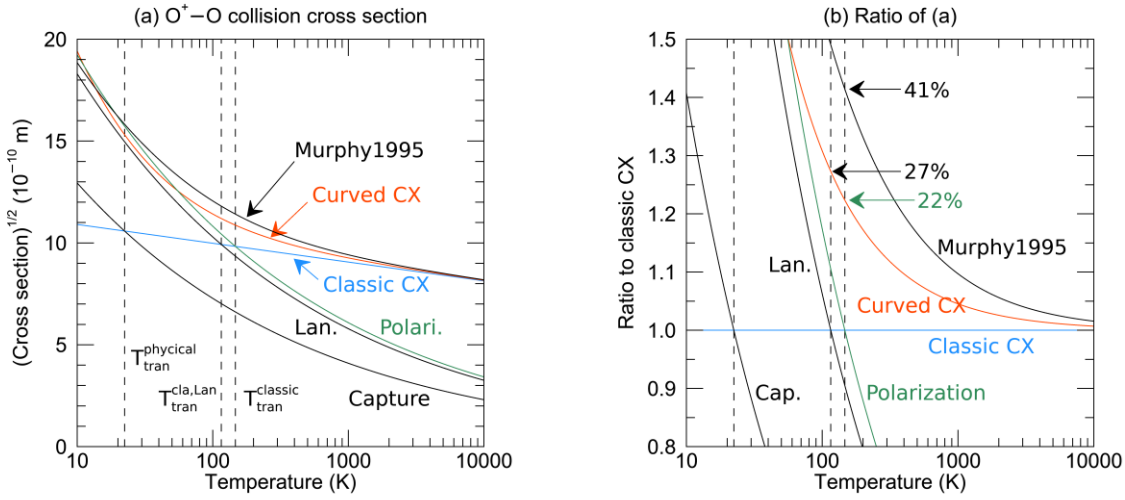

Figure 6. Components of temperature-dependent momentum-transfer collision cross sections. The O^+–O cross section model presented in Appendix B1 is used as an example. Most components are integrals of the energy-dependent components shown in Figure 5 and are shown similarly here, except that the prediction by Murphy (1995) is added. The dashed lines indicate transition temperatures. (a) Square-root of the momentum-transfer cross section. (b) Ratio of the components to the classic charge-exchange component. The effective charge-exchange component is higher than the greater of the polarization or classic charge-exchange components by at most 22%.

6 Derivation of Analytical Form

The effective temperature-dependent cross section was numerically obtained in the previous section. In this section, we derive the corresponding approximate analytical form.

6.1 Preparation

We prepare concise notation "< >" that represents the weighted averages, as explained in Appendix C. Using this notation, Equation 3-1 is generally expressed as

$$S_{\mathrm{MT}}\left(T_{\mathrm{r}}\right)=\frac{1}{2}\int_0^{\infty}Q_{\mathrm{MT}}x^2e^{-x}dx=\frac{1}{2}\left\langle Q_{\mathrm{MT}}x^2\right\rangle. \tag{6-1}$$

Equation 3-14 (i.e., $Q_{\mathrm{MT}}=2Q_{\mathrm{CX}}$) does not necessarily hold, but is used to define the MTCS that corresponds to CXCS in the following. We use the label str to explicitly indicate that the straight particle trajectory is assumed in CXCS:

$$S_{\mathrm{MT}}^{\mathrm{str}}\left(T_{\mathrm{r}}\right)=\frac{1}{2}\left\langle Q_{\mathrm{MT}}^{\mathrm{str}}x^2\right\rangle=\left\langle Q_{\mathrm{CX}}^{\mathrm{str}}x^2\right\rangle=2\times S_{\mathrm{CX}}^{\mathrm{str}}\left(T_{\mathrm{r}}\right). \tag{6-2}$$

In contrast, we use the label cv to explicitly indicate that the curve effect is included in CXCS:

$$S_{\mathrm{MT}}^{\mathrm{cv}}\left(T_{\mathrm{r}}\right)=\frac{1}{2}\left\langle Q_{\mathrm{MT}}^{\mathrm{cv}}x^2\right\rangle=\left\langle Q_{\mathrm{CX}}^{\mathrm{cv}}x^2\right\rangle=2\times S_{\mathrm{CX}}^{\mathrm{cv}}\left(T_{\mathrm{r}}\right). \tag{6-3}$$

6.2 General Form

Substitution of Equation 5-1 into Equation 6-3 yields

$$S_{\mathrm{CX}}^{\mathrm{cv}} = \frac{1}{2}\left\langle Q_{\mathrm{CX}}^{\mathrm{cv}} x^2 \right\rangle = \frac{1}{2}\left\langle Q_{\mathrm{CX}}^{\mathrm{str}} x^2 \right\rangle + \frac{1}{2}\left\langle \frac{1}{16}\frac{{Q_{\mathrm{Lan}}}^2}{Q_{\mathrm{CX}}^{\mathrm{str}}} x^2 \right\rangle = S_{\mathrm{CX}}^{\mathrm{str}} + \frac{1}{32}\left\langle \frac{{Q_{\mathrm{Lan}}}^2}{Q_{\mathrm{CX}}^{\mathrm{str}}} x^2 \right\rangle, \tag{6-4}$$

where Equation 6-2 was used.

From Equations 3-7 and 3-8, the energy- and temperature-dependent Langevin cross sections are related to each other by

$${Q_{\mathrm{Lan}}}^2 = \frac{C_{\mathrm{Lan}}}{w_{\mathrm{r}}} = \frac{C_{\mathrm{Lan}}}{x k_{\mathrm{B}} T_{\mathrm{r}}} = \frac{64}{9\pi}\frac{{S_{\mathrm{Lan}}}^2}{x}. \tag{6-5}$$

Accordingly, the second term (i.e., the curve effect) of Equation 6-4 is transformed as

$$S_{\mathrm{CX}}^{\mathrm{dcv}} \equiv \frac{1}{32}\left\langle {Q_{\mathrm{Lan}}}^2 \frac{x^2}{Q_{\mathrm{CX}}^{\mathrm{str}}} \right\rangle = \frac{1}{32}\left\langle \frac{64}{9\pi}\frac{{S_{\mathrm{Lan}}}^2}{x}\frac{x^2}{Q_{\mathrm{CX}}^{\mathrm{str}}} \right\rangle = \frac{2}{9\pi}{S_{\mathrm{Lan}}}^2 \left\langle \frac{x}{Q_{\mathrm{CX}}^{\mathrm{str}}} \right\rangle. \tag{6-6}$$

6.3 Approximate Form using a Typical Cross Section

Although Equation 6-6 can be numerically integrated, we aim to derive an analytical form. Direct analytical integration of $x/Q_{\mathrm{CX}}^{\mathrm{str}}$ in Equation 6-6 over energy is difficult and probably impossible. Thus, we approximate Equation 6-6 by replacing $Q_{\mathrm{CX}}^{\mathrm{str}}(\varepsilon_{\mathrm{r}})$ by a typical cross section $S_{\mathrm{CX}}^{\mathrm{typ}}(T_{\mathrm{r}})$ that is independent of energy but satisfies

$$\left\langle \frac{x}{Q_{\mathrm{CX}}^{\mathrm{str}}} \right\rangle \sim \left\langle \frac{x}{S_{\mathrm{CX}}^{\mathrm{typ}}} \right\rangle. \tag{6-7}$$

This approximation is numerically justified in the next section. This approximation is expected to be reasonable because only a limited range of x around the average normalized energy near $x \sim 2$ is practically relevant to Equation 6-6, owing to the exponential term in Equation 6-1. It is also reasonable because the energy dependence of $Q_{\mathrm{CX}}^{\mathrm{str}}(\varepsilon_{\mathrm{r}})$ is logarithmic, as shown in Equation 3-10, and thus is weaker than that of x.

Accepting this concept of approximation, Equation 6-7 can be transformed as

$$\left\langle \frac{x}{Q_{\mathrm{CX}}^{\mathrm{str}}} \right\rangle \approx \left\langle \frac{x}{S_{\mathrm{CX}}^{\mathrm{typ}}} \right\rangle = \frac{\langle x \rangle}{S_{\mathrm{CX}}^{\mathrm{typ}}} = \frac{1}{S_{\mathrm{CX}}^{\mathrm{typ}}}. \tag{6-8}$$

Accordingly, the curve effect in Equation 6-6 is approximated as

$$S_{\mathrm{CX}}^{\mathrm{dcv}} = \frac{2}{9\pi}{S_{\mathrm{Lan}}}^2 \left\langle \frac{x}{Q_{\mathrm{CX}}^{\mathrm{str}}} \right\rangle \approx \frac{2}{9\pi}\frac{{S_{\mathrm{Lan}}}^2}{S_{\mathrm{CX}}^{\mathrm{typ}}} = \frac{\alpha_{\mathrm{V}}}{S_{\mathrm{CX}}^{\mathrm{typ}} T_{\mathrm{r}}} 1.0312 \times 10^{-5}, \tag{6-9}$$

where Equation 3-8 was used. The corresponding effective cross section in Equation 6-4 is

$$S_{\mathrm{CX}}^{\mathrm{cv}} \approx S_{\mathrm{CX}}^{\mathrm{str}} + S_{\mathrm{CX}}^{\mathrm{dcv}} = S_{\mathrm{CX}}^{\mathrm{str}} + \frac{2}{9\pi}\frac{{S_{\mathrm{Lan}}}^2}{S_{\mathrm{CX}}^{\mathrm{typ}}} = S_{\mathrm{CX}}^{\mathrm{str}} + \frac{\alpha_{\mathrm{V}}}{S_{\mathrm{CX}}^{\mathrm{typ}} T_{\mathrm{r}}} 1.0312 \times 10^{-5}. \tag{6-10}$$

7 Selection of Typical Cross Section

We have derived an approximate analytical form of the effective CXCS in Equation 6-10. In this form, the concept of typical CXCS $S_{\mathrm{CX}}^{\mathrm{typ}}(T_{\mathrm{r}})$ is introduced to avoid numerical integration of the curve effect. Four actual expressions of $S_{\mathrm{CX}}^{\mathrm{typ}}$ are evaluated in this section. All types can be useful depending on the relative importance of accuracy and simplicity. We recommend the factored type for typical application.

7.1 Simple Average-Energy Type

A quick candidate for $S_{\mathrm{CX}}^{\mathrm{typ}}(T_{\mathrm{r}})$ is the classic temperature-dependent CXCS $S_{\mathrm{CX}}^{\mathrm{str}}(T_{\mathrm{r}})$ in Equation 3-13. That is, we assume

$$S_{\mathrm{CX}}^{\mathrm{typ}} = S_{\mathrm{CX}}^{\mathrm{str}} \tag{7-1}$$

in Equation 6-9.

This type is evaluated in Figure 7a as follows. We first calculate the curve component $S_{\mathrm{CX}}^{\mathrm{dcv}}(T_{\mathrm{r}})$ using the numerical integration in Equation 6-6. The results are expected to be accurate and are used as references. We then calculate the curve component using Equation 7-1 (i.e., simple type) in Equation 6-9. The resultant $S_{\mathrm{CX}}^{\mathrm{dcv}}(T_{\mathrm{r}})$ are compared with the reference values by taking the difference.

This comparison was conducted for three sets of A_0/B_0. The classic CXCS is characterized by constants A_0 and B_0, as shown in Equation 3-12. Our example O^+–O collision model in Appendix D corresponds to $A_0 \sim 6$ and $A_0/B_0 \sim 9$, which is used as the primary test. The ratio A_0/B_0 is relatively constant and is typically between 8 and 10 among the particle pairs that are relevant to ionospheric studies in Banks (1966). Accordingly, we also tested the cases with $A_0/B_0 = 6$ and 12 as measures of maximum deviation. The constant A_0 is fixed at 6 because its variation is not essential in this test of the replacement of numerical integration.

The three sets of A_0/B_0 correspond to the three lines in Figure 7a1. The resultant difference in $S_{\mathrm{CX}}^{\mathrm{dcv}}(T_{\mathrm{r}})$ is relatively small and typically within 4%. Figure 7a2 shows the corresponding difference in the total (classic plus curve) charge-exchange component $S_{\mathrm{MT}}^{\mathrm{cv}}(T_{\mathrm{r}})$, which is much lower and within 1% accuracy at temperatures above the classic-type transition temperature of 146.8 K. Accordingly, this simple type is reasonably accurate, especially above approximately the classic transition temperature, in terms of the difference from the numerically integrated values.

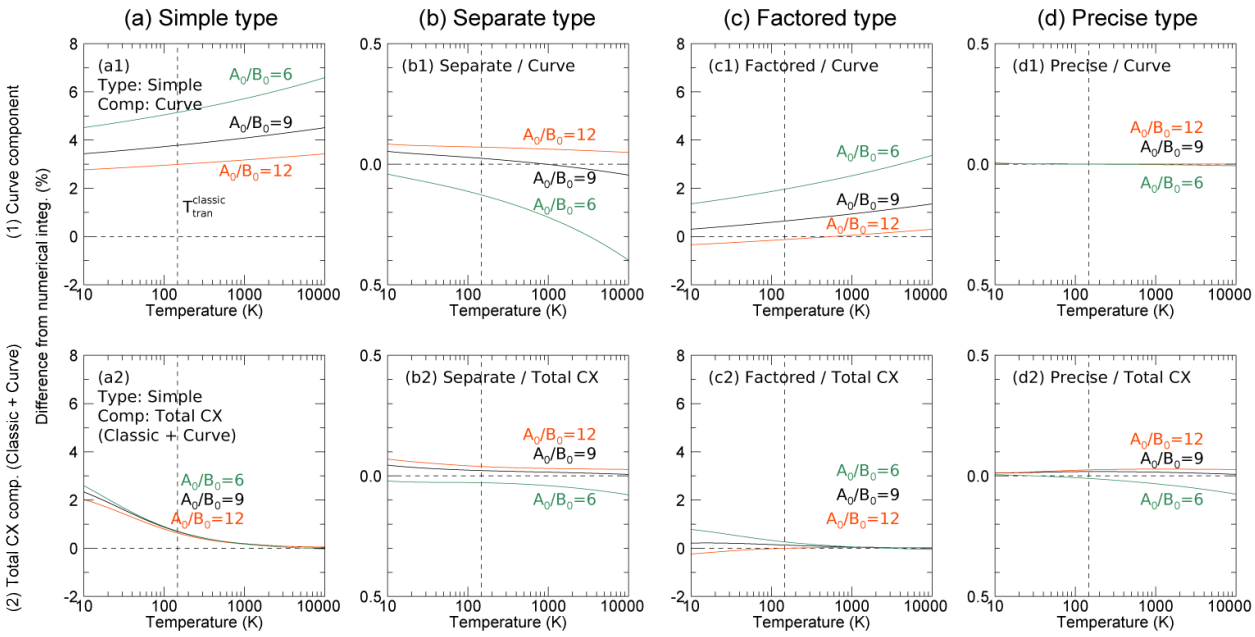

Figure 7. Four candidates for the typical cross section are evaluated by difference from accurate numerical integration. The O^+–O cross section model presented in Appendix B1 is used as an example. The typical cross sections are used to replace numerical integration of the curve effect over energy in this study. The upper and lower panels respectively show the difference in the curve component $S_{\mathrm{CX}}^{\mathrm{dcv}}(T_{\mathrm{r}})$ and the total (classic plus curve) charge-exchange component $S_{\mathrm{CX}}^{\mathrm{cv}}(T_{\mathrm{r}})$. From left to right shown are four types of typical cross sections: (a) simple, (b) separate, (c) factored, and (d) precise. The constants A_0 and B_0 characterize the classic-type CXCS in Equation 3-12. The three lines in each panel correspond to A_0/B_0 ratios of 6, 9, and 12. The constant A_0 is always fixed at 6. The dashed lines indicate the classic transition temperatures.

7.2 Separate Average-Energy Type

It is unclear what is the source of the small error in the simple average-energy type in Figure 7a. Accordingly, we attempt to find a more accurate approximation of numerical integration.

The classic CXCS in Equation 3-13 can be interpreted as

$$S_{\mathrm{CX}}^{\mathrm{str}}\left(T_{\mathrm{r}}\right)=\left[A_0-B_0\log_{10}\left(X_{\mathrm{a}}\times T_{\mathrm{r}}k_{\mathrm{B}}/e\right)\right]^2, \tag{7-2}$$

where $X_{\mathrm{a}} \sim 2.492$. That is, this classic temperature-dependent CXCS implies that the variable normalized energy $x = e\varepsilon_{\mathrm{r}}/k_{\mathrm{B}}T_{\mathrm{r}}$ in the classic energy-dependent CXCS $Q_{\mathrm{CX}}^{\mathrm{str}}(\varepsilon_{\mathrm{r}})$ in Equation 3-12 is replaced by the constant average normalized energy $X_{\mathrm{a}} \sim 2.492$.

Equation 7-1 implies that X_{a} is assumed to be 2.492 for the typical cross section in the simple average-energy type. However, X_{a} should differ from 2.492 for the typical cross section. Thus, the approximation is expected to be improved if another average normalized energy $X_{\mathrm{a}}^{\mathrm{typ}}$ is separately used for the typical cross section as

$$S_{\mathrm{CX}}^{\mathrm{typ}}\left(T_{\mathrm{r}}\right)=\left[A_0-B_0\log_{10}\left(X_{\mathrm{a}}^{\mathrm{typ}}\times T_{\mathrm{r}}k_{\mathrm{B}}/e\right)\right]^2. \tag{7-3}$$

We calculate this another X_a^{typ} inversely as follows. We first calculate the correct $S_{CX}^{dcv}(T_r)$ by numerical integration in Equation 6-6. Inserting this $S_{CX}^{dcv}(T_r)$ in Equation 6-9 yields

$$S_{CX}^{typ} \approx \frac{2}{9\pi}\frac{S_{Lan}{}^2}{S_{CX}^{dcv}}. \tag{7-4}$$

Then, substituting into Equation 7-3 yields the resultant $X_a^{typ}(T_r, B_0/A_0)$.

Figure 8a shows the map of the resultant average normalized energy $X_a^{typ}(T_r)$ for three different A_0/B_0 ratios. This quantity appears to be approximately 1.59, which corresponds to $A_0/B_0 = 9$ at 1000 K, as shown in Figure 8a. Deviations in X_a^{typ} from 1.59 appear to be typically 0.04, which is much smaller than the difference (0.9) from $X_a \sim 2.492$, which corresponds to the classic cross section. Accordingly, the typical cross section is expected to be improved by replacing $X_a = 2.492$ with $X_a^{typ} = 1.59$. That is,

$$S_{CX}^{typ} \sim \left[A_0 - B_0 \log_{10}\left(1.59 \times k_B T_r / e\right)\right]^2 \approx \left[A_0 + B_0\left(3.86 - \log_{10} T_r\right)\right]^2. \tag{7-5}$$

This expectation is confirmed by the curves shown in Figure 7b, which are shown similarly to the simple type in Figure 7a. The difference in the curve component is within 0.4% and is typically 0.1% in Figure 7b1, which is much smaller than that in Figure 7a1 (4%). The difference in the corresponding total (classic plus curve) charge-exchange component $S_{MT}^{cv}(T_r)$ is 0.1% in Figure 7b2, which is much smaller than approximately 1% in Figure 7a2. In summary, the error in the simple type is mostly due to the fact that the average energy of the classic charge exchange is implicitly used in the typical cross section. The simple type is improved by adoption of the average energy of the typical cross section to become the separate type.

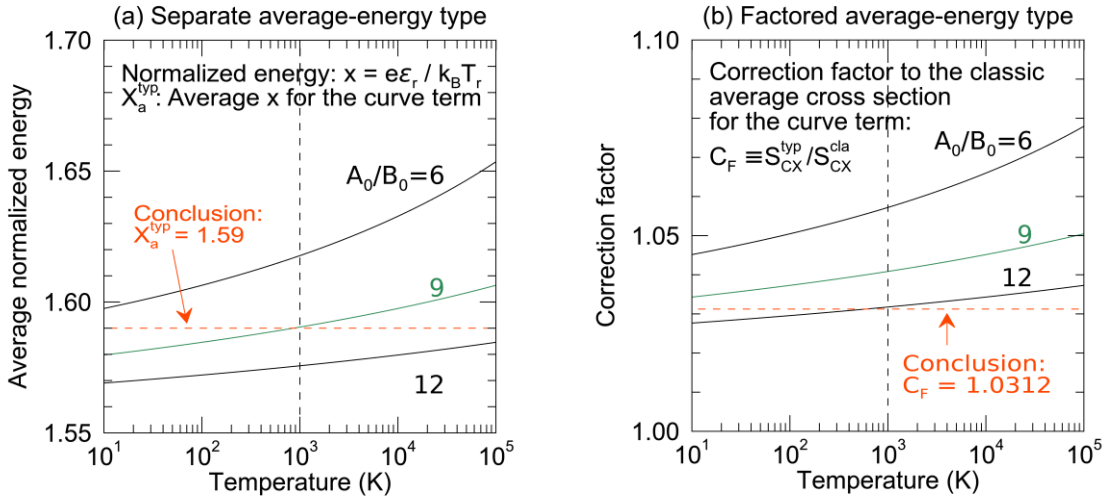

Figure 8. Quantities that characterize typical cross section candidate models. The O^+–O cross section model presented in Appendix B1 is used as an example. The characteristic quantities are calculated from the consistency with the correct values obtained by numerical integration of the curve effect. The characteristic quantities corresponding to three A_0/B_0 ratios are shown. The A_0/B_0 ratio characterizes the charge-exchange collision. A_0 is fixed at 6. The characteristic quantities are then approximated to be constant in this figure to construct typical cross section

models, which are used to skip the numerical integration of the curve effect. (a) Separate average-energy type in Equation 7-3 and (b) factored average-energy type in Equation 7-6.

7.3 Factored Average-Energy Type

The separate type is an improvement on the simple type, but it requires an additional Equation 7-5 and thus is not very concise. The simple type may be improved in a different way. We expect that $S_{\mathrm{CX}}^{\mathrm{typ}}$ is reasonably proportional to the classic CXCS with a constant factor,

$$S_{\mathrm{CX}}^{\mathrm{typ}} = C_{\mathrm{F}} S_{\mathrm{CX}}^{\mathrm{str}} . \tag{7-6}$$

This factor C_{F} is also calculated inversely, similar to X_a in Section 7.2. Figure 8b shows a map of the resultant factor. This factor is approximately 1.04 at 1000 K, as shown in Figure 8b. We conservatively approximate that this factor is approximately 1.0312 so that Equation 6-10 is approximated to be a simple form:

$$S_{\mathrm{CX}}^{\mathrm{cv}} \approx S_{\mathrm{CX}}^{\mathrm{str}} + \frac{\alpha_{\mathrm{V}} \times 10^{-5}}{S_{\mathrm{CX}}^{\mathrm{str}} T_{\mathrm{r}}} . \tag{7-7}$$

We evaluate this factored type approximation similar to that in Section 7.2. Figure 7c1 shows the difference in $S_{\mathrm{CX}}^{\mathrm{dcv}}(T_{\mathrm{r}})$. The difference is within 2% and is somewhat smaller than that in Figure 7a1 (4%). The difference in $S_{\mathrm{CX}}^{\mathrm{cv}}(T_{\mathrm{r}})$ in Figure 7c2 is typically three times smaller than that in Figure 7a2 and is within 1%. In addition, the resultant Equation 7-7 is simple. Thus, we recommend this factored type for typical ionospheric applications.

7.4 Precise Taylor Expansion Type

A precise form of the typical cross section is obtained in Appendix E using the Taylor expansion and gamma functions. This option is evaluated similarly, as shown in Figure 7d. The difference in $S_{\mathrm{CX}}^{\mathrm{dcv}}(T_{\mathrm{r}})$ is less than 0.01% and is difficult to see visually in Figure 7d1. The small difference justifies our approximation in Equation 6-7.

Figure 7d2 shows a similar comparison, but for the total charge-exchange component in $S_{\mathrm{CX}}^{\mathrm{cv}}(T_{\mathrm{r}})$. The difference is less than 0.1%, but it is larger than the difference in Figure 7d1. The larger difference implies that it does not stem from the assumption Equation 6-7, but rather from the small error in approximation in the integration of the classic component in Equation 3-13, which is detailed in Appendix D. This precise type is used as a reference in this study, but may not be concise enough for typical ionospheric studies.

8 Discussion

8.1 Switching of the Two Domains

We have obtained an approximate form to express the curved or effective CXCS in Equation 6-10. This CXCS is multiplied by a factor of two as in Equation 3-14 to obtain the corresponding MTCS. The resultant MTCS can be recognized as the total MTCS above approximately the classic transition temperature $T_{\mathrm{tran,cla}}$. However, the total MTCS should instead approach the polarization component as the temperature decreases.

The energy-dependent curved MTCS is numerically the same as the Langevin cross section at the physical transition energy in Figure 5a. In contrast, the temperature-dependent curved MTCS is larger than the Langevin cross section by 4% at the physical transition temperature in Figure 9a because the temperature-dependent cross section is the average of the energy-dependent cross section. The curved MTCS is the closest to the Langevin cross section near the physical transition temperature $T_{\text{tran,phy}}$ defined in Equation 4-5. Therefore, this definition is numerically reasonable.

There is a temperature where the curved MTCS intersects the polarization cross section in Figure 9a. We call this temperate the switching temperature T_{switch} between the physical and classic temperatures as

$$T_{\text{tran}}^{\text{phy}} < T_{\text{switch}} < T_{\text{tran}}^{\text{cla}}. \tag{8-1}$$

The total MTCS can be generally expressed by the polarization cross section below T_{switch} and by the curved MTCS above T_{switch}:

$$S_{\text{MT}}^{\text{total}} \sim \begin{cases} S_{\text{pol}} & \left(T_{\text{r}} < T_{\text{switch}},\ \text{i.e., in the polarization domain}\right) \\ S_{\text{MT}}^{\text{cv}} & \left(T_{\text{r}} > T_{\text{switch}},\ \text{i.e., in the curved charge-exchange domain}\right) \end{cases}. \tag{8-2}$$

However, T_{switch} is generally much lower than $T_{\text{tran,cla}}$. This means that the polarization domain is less relevant to the ionosphere in the revised regime than it had been in the classic regime. Accordingly, Equation 8-2 can usually be simplified in actual computation, as summarized in Appendix B.

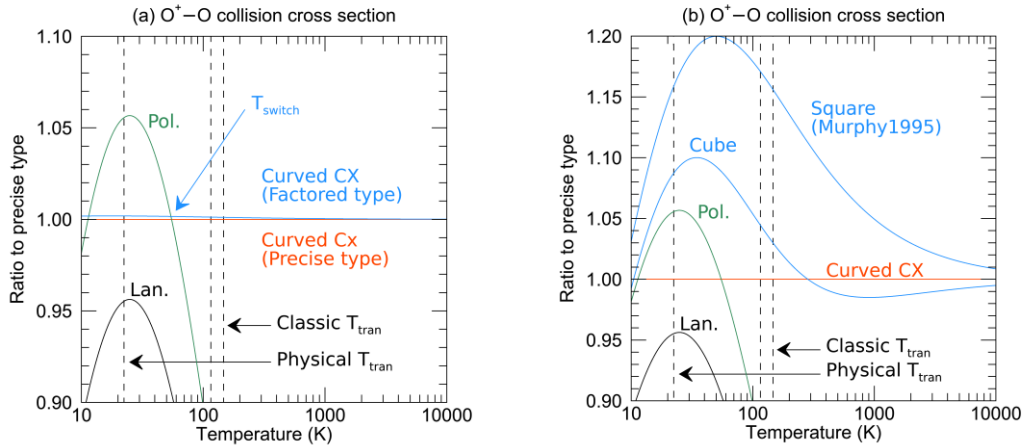

Figure 9. Components of temperature-dependent momentum-transfer collision cross sections. The O^+–O cross section model presented in Appendix B1 is used as an example. Shown are ratios in a format similar to that of Figure 6b, except that reference values are the precise type curved charge-exchange component labeled curved CX (precise type). (a) The switching temperature is indicated. (b) The Murphy (1995) model is shown. We point out that another model labeled cube is closer to the correct values (i.e., the polarization component at low temperatures and curved charge-exchange component at high temperatures).

8.2 Murphy Form

As mentioned in Section 1, the total MTCS has been estimated as the root-mean-square of the polarization and the classic-type charge-exchange components in some previous studies (e.g., Capitelli et al., 2013; Laricchiuta et al., 2009; Wright et al., 2007; Murphy, 1995, 2000, 2012); that is,

$$S_{\mathrm{MT}}^{\mathrm{total}} \equiv \sqrt{\left(S_{\mathrm{pol}}\right)^2 + \left(S_{\mathrm{MT}}^{\mathrm{str}}\right)^2}\ , \tag{8-3}$$

as shown by the line labeled Murphy1995 in Figure 6. The corresponding maximum enhancement is 41% by definition, that is, $\sqrt{2} - 1$. This value significantly overestimates the precise value (22%). We could not find a reasoning for this form in these studies. Thus, Equation 8-3 probably has no physical implications.

However, this form is simple because it does not require the consideration of transition temperatures. Thus, this form would be useful if the physical implication is not important. In this case, the cube-mean

$$S_{\mathrm{MT}}^{\mathrm{total}} \equiv \left[\left(S_{\mathrm{pol}}\right)^3 + \left(S_{\mathrm{MT}}^{\mathrm{str}}\right)^3\right]^{1/3} \tag{8-4}$$

is also simple and is numerically much better than Equation 8-3, as can be seen in Figure 9b. In particular, differences from the precise type cross section are at most 3% above the classic transition temperature whereas the corresponding difference can be 15% in Equation 8-3. Thus, we propose to replace Equation 8-3 by Equation 8-4.

8.3 Why Is Enhancement Neglected in Classic Studies?

The enhancement has been neglected in ionospheric studies partly because of the following confusion. Banks (1966) showed a line that indicates the total cross section in Figure 1 (their Figure 2). They neglected the enhancement in the total cross section because they recognized that "the maximum error arising from the omission of the polarization effect is 11 per cent" (p. 1115) for the O^+–O collision. However, they did not explain how they calculated this 11% and the total cross section. Instead, they referred to Knof et al. (1964).

Knof et al. (1964) showed a similar line that indicates the total cross section in their Figure 4. They determined the line by "graphical interpolation between the high and low temperature asymptotes" (p. 3551). They did not explain what "graphical interpolation" means, except for referring to Mason and Vanderslice (1959), who made no explanation but stated that this "graphical interpolation" is "reasonably accurate" (p. 500).

Although we cannot find explicit explanations in the literature, this "graphical interpolation" probably does not refer to a state-of-the-art graphical theory but rather to a less-strict manual visual expectation. Such an interpolation can have significant ambiguity without a reference value. Accordingly, we speculate that there was an unstated reference value to conduct the "graphical interpolation" in Banks (1966), Knof et al. (1964), and Mason and Vanderslice (1959).

The maximum enhancement is 25% for the energy-dependent cross section in Equation 5-2 when the Langevin component is referenced. This number may have been known in some previous studies (e.g., Heiche & Mason, 1970) because Equation 5-2 is known. The maximum

enhancement is expected to be similar in the temperature-dependent cross section because this cross section originates from the energy-dependent cross section. Thus, prediction by "graphical interpolation" should be "reasonably accurate" if the enhancement in the energy-dependent cross section is implicitly referred to. This is probably what Mason and Vanderslice (1959) intended to state.

This expectation is confirmed to be reasonable in the present study; that is, the maximum enhancement in the temperature-dependent cross section from the Langevin cross section is 27.3%, which is close to the 25% in the energy-dependent cross section. In other words, the present study has derived a function that is practically equivalent to "graphical interpolation."

However, it is still unclear why the maximum enhancement was 11% in Banks (1966), which is significantly lower than 25%. A key to resolve this discrepancy is that this 11% is close to 10.5%, which has been known as the classic glancing particle contribution to the polarization collision in Equation 3-10. That is, Banks (1966) have presumably confused the classic glancing contribution with the curve effect on the charge-exchange component.

It should be noted that the classic glancing particles are located outside the orbiting radius and thus are not captured. In contrast, for the parental particle pair, a charge-exchange reaction area is added. Then, some of the glancing particles hit this additional area. Consequently, the glancing polarization collision becomes the head-on charge-exchange collision. Accordingly, the momentum transfer is significantly enhanced. This curve effect is much larger than the classic glancing contribution.

In summary, the enhancement has been neglected in ionospheric studies, partly due to the confusion about the glancing contribution in Banks (1966). Setting aside the confusion, this neglect may have been a practical compromise to express the temperature-dependent cross section because there was no temperature-dependent functional form to express the enhancement. This functional form has been derived in the present study. Thus, there is no longer any reason to ignore the enhancement, which is at most 22% when the polarization component is referenced. The computational details are summarized in Appendix A.

9 Conclusion

We have studied the ion–neutral collision cross section or frequency for a parental particle pair such as O^+–O. Collisions of such parental pairs include polarization and charge-exchange components. The coupling of the two components has been ignored in the classic straight-trajectory regime, partly due to confusion with the glancing component.

In contrast, we include the coupling, which is the curved trajectory effect on the charge-exchange component. In this curved-trajectory regime, the collision cross section or frequency is generally enhanced by approximately 22% at the maximum. We derived a simple form that expresses the enhancement as a function of temperature for practical application.

There may be additional effects on the collision frequency, depending on the particle pair. For example, the fine-structure effect works for the O^+–O collision. This effect will be investigated in a separate study.

Appendix A: Summary of Computation

In this appendix, analytical forms of the collision cross section and frequency are summarized for computation. The curve effect is included to improve the classic form. Physical units are defined in Section 2. This summary is valid only for collisions between ions and their parent neutral particles, such as O^+ and O. Note that the factored-type typical cross section is adopted here but the other three typical cross sections derived in Section 7 could be used instead, depending on the relative importance of accuracy and simplicity.

A1 Input Parameters and Classic Cross Sections

There are two input parameters: (1) the dipole polarizability volume α_V (m^3) in Equation 3-5, which is used in Equations 3-8 and 3-10 to obtain the Langevin and polarization cross sections; and (2) the charge-exchange constants A_0 and B_0, which are defined with the classic (i.e., without the curve effect) CXCS $Q_{CX}^{str}(\varepsilon_r)$ (m^2) in Equation 3-12 as

$$Q_{CX}^{str}\left(\varepsilon_r\right) = \left(A_0 - B_0 \log_{10} \varepsilon_r\right)^2 . \tag{A-1}$$

These input parameters yield classic-type cross sections in Section 3 as

$$\begin{cases} S_{pol} = 1.105 \times S_{Lan} \approx 1.105 \times 0.01207148 \sqrt{\alpha_V / T_r} \approx 0.013339 \sqrt{\alpha_V / T_r} \\ S_{CX}^{str} \sim \left[A_0 + B_0 \left(3.668 - \log_{10} T_r\right)\right]^2 \end{cases} . \tag{A-2}$$

A2 Effective Collision Cross Section and Frequency

The curved or effective CXCS is generally approximated as Equation 6-10. Substituting the factored-type typical cross section in Equation 7-7 yields

$$S_{CX}^{cv}\left(T_r\right) \sim S_{CX}^{str} + \frac{2}{9\pi} \frac{{S_{Lan}}^2}{S_{CX}^{typ}} \approx S_{CX}^{str} + \frac{\alpha_V \times 10^{-5}}{S_{CX}^{typ} T_r} 1.0312 = S_{CX}^{str} + \frac{\alpha_V \times 10^{-5}}{S_{CX}^{str} T_r} . \tag{A-3}$$

The total MTCS is generally obtained using Equation 8-2, which can usually be simplified in realistic ionospheric temperatures as

$$S_{MT}^{total}\left(T_r\right) = \max\left(S_{pol}, 2 \times S_{CX}^{cv}\right), \tag{A-4}$$

where the max operator indicates the greater of the two coefficients (i.e., the polarization or charge-exchange here) for each temperature. Note that Equation A-4 is invalid at extremely low temperatures (e.g., less than 11 K in Figure 9a).

The collision frequency can be calculated using Equation 3-3. Approximating the ion mass to be the same as the neutral mass,

$$\nu_{in,LAB} / n_n \sqrt{T_r} S_{MT}^{total} \sim \frac{1}{2} \frac{4}{3} \sqrt{\frac{8 k_B}{\pi m_u A_r / 2}} \sim \frac{137.19}{\sqrt{A_r}} . \tag{A-5}$$

Using Equations A-2 and A-4,

$$\nu_{in,LAB} / n_n \sim \frac{137.19}{\sqrt{A_r}} \sqrt{T_r} \times \max\left(0.013339 \sqrt{\frac{\alpha_V}{T_r}}, 2 \times S_{CX}^{cv}\right) = \max\left(1.8299 \sqrt{\frac{\alpha_V}{A_r}}, \frac{274.37}{\sqrt{A_r}} S_{CX}^{cv} \sqrt{T_r}\right) . \tag{A-6}$$

Appendix B: Example O^+–O Model

An example O^+–O collision model was used in this study. Equations specific to this model are summarized as example usage of Appendix A.

B1 Input Parameters and Classic Cross Sections

Atomic oxygen has a relative atomic mass A_r of 16.0. The dipole polarizability volume of an oxygen atom is $\alpha_V = 0.77 \times 10^{-30}$ m^3 from Table 1 of Alpher and White (1959), Table 4.1 of Schunk and Nagy (2009), and Table B1 of Ieda (2020).

We use the O^+–O charge-exchange collision model proposed by Ieda (2021). This model is based on Stebbings et al. (1964), who conducted an ion-beam experiment to measure the energy-dependent CXCS of O^+–O collision at 40–10,000 eV. Their experiment was contaminated with excited-state O^+, and their results were adjusted by Ieda (2021) to the ground-state O^+-only case. The resultant model is characterized by charge-exchange constants

$$\begin{cases} A_0\left[\mathrm{m}\right] = 5.9700\times10^{-10} \\ B_0\left[\mathrm{m}\right] = 0.65292\times10^{-10} \end{cases}, \tag{B-1}$$

which are defined with Equation A-1.

Corresponding classic-type cross sections are obtained using Equation A-2 as

$$\begin{cases} S_{\mathrm{pol}}\left[\mathrm{m}^2\right] = 0.013339\sqrt{0.77\times10^{-30}\,/\,T_{\mathrm{r}}} = 1170.5\times10^{-20}\,/\,\sqrt{T_{\mathrm{r}}} \\ S_{\mathrm{CX}}^{\mathrm{str}}\left[\mathrm{m}^2\right] = \left(8.3648 - 0.65292\times\log_{10}T_{\mathrm{r}}\right)^2\times10^{-20} \end{cases}. \tag{B-2}$$

B2 Effective Collision Cross Section and Frequency

Using the input polarization volume, the curved or effective CXCS in Equation A-3 yields

$$S_{\mathrm{CX}}^{\mathrm{cv}} \sim S_{\mathrm{CX}}^{\mathrm{str}} + \frac{0.77\times10^{-35}}{S_{\mathrm{CX}}^{\mathrm{str}}T_{\mathrm{r}}}, \tag{B-3}$$

where the classic cross section $S_{\mathrm{CX}}^{\mathrm{str}}(T_{\mathrm{r}})$ is given by Equation B-2. Note that the factored-type typical cross section is adopted in Equation A-3.

Equation A-6 corresponds to

$$\nu_{\mathrm{in,LAB}} / n_{\mathrm{n}} \sim \max\left(1.8299\sqrt{\frac{0.77\times10^{-30}}{16.0}}, \frac{274.37}{\sqrt{16.0}}S_{\mathrm{CX}}^{\mathrm{cv}}\sqrt{T_{\mathrm{r}}}\right) = \max\left(4.014\times10^{-16}, 68.593\sqrt{T_{\mathrm{r}}}S_{\mathrm{CX}}^{\mathrm{cv}}\right).$$

However, the switching temperature of this particular O^+–O collision is 54 K, which is lower than the ionospheric temperature range; thus, Equation B-4 reduces to

$$\nu_{\mathrm{in,LAB}} / n_{\mathrm{n}} = 68.593\sqrt{T_{\mathrm{r}}}S_{\mathrm{CX}}^{\mathrm{cv}}. \tag{B-5}$$

Appendix C: Gamma Functions

The gamma function is used for semi-analytical integration of energy-dependent cross sections in this study. The specific values are summarized in this appendix. The gamma function is defined as

$$\Gamma(z) = \int_0^\infty x^{z-1} e^{-x} dx \tag{C-1}$$

and its derivatives are

$$\frac{d^n \Gamma(z)}{dz^n} = \int_0^\infty x^{z-1} (\ln x)^n e^{-x} dx \tag{C-2}$$

For concise form, we define an operator for quantity y as

$$\langle y \rangle = \int_0^\infty y e^{-x} dx . \tag{C-3}$$

We calculate some values associated with gamma functions using the method outlined by Mason and Vanderslice (1959) as follows:

$$\begin{cases} \langle x \rangle = \int_0^\infty x e^{-x} dx = \Gamma(2) = 1 \\ \langle x^{3/2} \rangle = \int_0^\infty x^{3/2} e^{-x} dx = \Gamma(5/2) = \frac{3}{4}\sqrt{\pi} \\ \langle x^2 \rangle = \int_0^\infty x^2 e^{-x} dx = \Gamma(3) = 2 \\ \langle x^3 \rangle = \int_0^\infty x^3 e^{-x} dx = \Gamma(4) = 6 \\ \langle x \ln x \rangle = \int_0^\infty x (\ln x)^3 e^{-x} dx = \Gamma'(2) \approx 0.42277 \\ \langle x (\ln x)^2 \rangle = \int_0^\infty x (\ln x)^2 e^{-x} dx = \Gamma''(2) \approx 0.82371 \\ \langle x (\ln x)^3 \rangle = \int_0^\infty x (\ln x)^3 e^{-x} dx = \Gamma'''(2) \approx 0.59248 \end{cases} . \tag{C-4}$$

Appendix D: Small Adjustment to Classic Charge-Exchange Cross Section

In this appendix, we detail a small adjustment to the classic temperature-dependent CXCS in Section 3.5. This adjustment improves the classic CXCS in ionospheric studies. The improvement is typically 0.1%, which is usually negligible, except in detailed studies such as this one, which evaluates numerical integrations in Section 7.4.

The classic energy-dependent CXCS in Equation 3-12 is often given by theoretical study or laboratory experiment as

$$Q_{CX}(\varepsilon_r) = (A_0 - B_0 \log_{10} \varepsilon_r)^2 . \tag{D-1}$$

The corresponding temperature-dependent CXCS can be obtained using gamma functions in Equation C-4, as outlined by Mason and Vanderslice (1959), as

$$S_{CX}(T_r) \sim \left[A_0 - B_0 \log_{10} (2.5163 \times T_r k_B / e) \right]^2 + 0.074489 \times B_0^{\,2} , \tag{D-2}$$

which is consistent with Equation 7 of Pesnell et al. (1994).

The last term is usually neglected, as in Pesnell et al. (1994), resulting in

$$S_{\mathrm{CX}}(T_{\mathrm{r}}) \sim \left[A_0 - B_0 \log_{10}\left(X_{\mathrm{a}} \times T_{\mathrm{r}} k_{\mathrm{B}} / e\right)\right]^2 = \left[A_0 + B_0\left(R_{\mathrm{T}} - \log_{10} T_{\mathrm{r}}\right)\right]^2, \tag{D-3}$$

where $X_a \approx 2.5163$ and $R_T \approx 3.664$, which is consistent with Equation 26 of Banks (1966) and Equation 4.151 of Schunk and Nagy (2009).

However, the last term (~$0.07 \times B_0^2$) in Equation D-2 is always positive. Accordingly, Equation D-3 always underestimates. This underestimation is typically 0.1% in ionospheric applications, as shown in Figure D1a.

We make a small adjustment to R_{T} in Equation D-3 to compensate for dropping the last term of Equation D-2 as follows. The correct S_{CX} is obtained in Equation D-2 and inserted into Equation D-3 to obtain the corresponding equivalent R_{T}. The resultant R_{T} values are shown in Figure D1c and is closer to 3.668 than to the classic value of 3.664.

Thus, we replace $R_T \approx 3.664$ in Equation D-3 with $R_T \equiv 3.668$ to obtain

$$S_{\mathrm{CX}}(T_{\mathrm{r}}) \equiv \left[A_0 + B_0 \times \left(3.668 - \log_{10} T_{\mathrm{r}}\right)\right]^2 \approx \left[A_0 - B_0 \log_{10}\left(2.492 \times T_{\mathrm{r}} k_{\mathrm{B}} / e\right)\right]^2. \tag{D-4}$$

The corresponding difference from Equation D-2 is shown in Figure D1b. The temperature range between 100 and 10,000 K includes Earth's ionosphere and Solar chromosphere. The resultant error is typically 0.02% and is much smaller in Figure D1b than in Figure D1a.

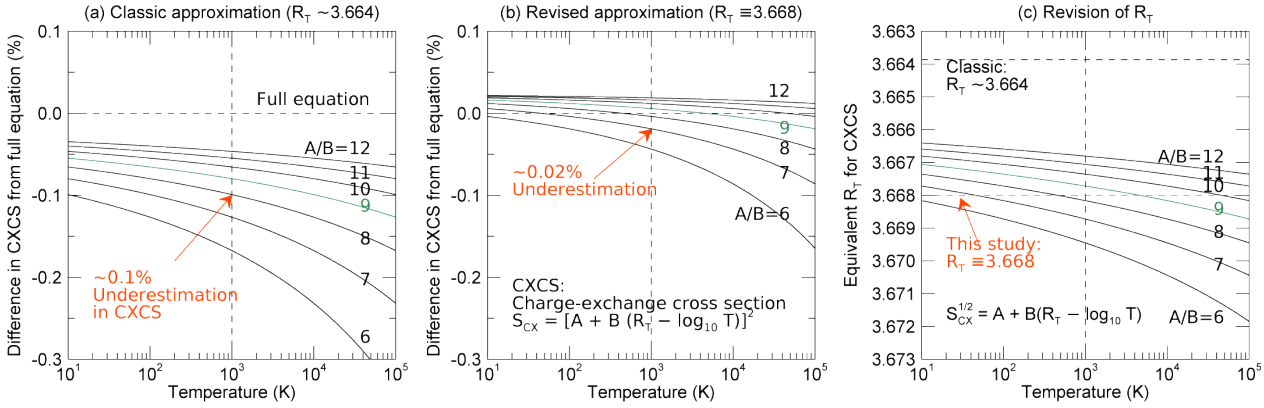

Figure D1. Small adjustment in classic temperature-dependent charge-exchange cross section (CXCS) or collision frequency. The classic temperature-dependent CXCS originally includes a small term (~$0.07 \times B_0^2$) in Equation D-2. This term is neglected in Equation D-3, as in Schunk and Nagy (2009). (a) Original difference from Equation D-2 of Equation D-3. (b) Reduced difference from Equation D-2 of modified version of Equation D-3, where the neglection of the small term is partly compensated by the adjustment of the factor R_{T} from 3.664 to 3.668. (c) The equivalent factor R_{T} that makes Equation D-3 consistent with Equation D-2. The resultant value R_{T} = 3.668 is used in (b).

Appendix E: Derivation of Precise Typical Charge-Exchange Cross Section for the Curve Effect

In Section 6, we derive an approximate analytical form of the temperature-dependent CXCS including the curve effect in Equation 6-10. This form requires a typical CXCS that satisfies Equation 6-7. Three types of approximate typical CXCS are derived in Section 7. In this

appendix, we derive another typical CXCS using Taylor expansions. The result is the most precise but is less concise.

At each temperature, using the normalized energy x in Equation 3-2, the energy-dependent CXCS in Equation 3-12 can be transformed as follows:

$$\sqrt{Q_{\mathrm{CX}}^{\mathrm{str}}} = A_0 - B_0 \log_{10} \varepsilon_{\mathrm{r}} = A_0 - B_0 \log_{10} \left(x k_{\mathrm{B}} T_{\mathrm{r}} / e \right) = A_0 - B_0 \log_{10} \left(k_{\mathrm{B}} T_{\mathrm{r}} / e \right) - B_0 \log_{10} x \,. \tag{E-1}$$

We define the following for brevity:

$$\begin{cases} A_{\mathrm{T}} \equiv A_0 - B_0 \log_{10} \left(k_{\mathrm{B}} T_{\mathrm{r}} / e \right) = A_0 + B_0 \left(4.0646 - \log_{10} T_{\mathrm{r}} \right) \\ \beta_{\mathrm{T}} \equiv B_0 \left(\log_{10} e \right) / A_{\mathrm{T}} \\ y \equiv \beta_{\mathrm{T}} \ln x \end{cases} . \tag{E-2}$$

Then, Equation E-1 is expressed as

$$\sqrt{Q_{\mathrm{CX}}^{\mathrm{str}}} = A_{\mathrm{T}} - B_0 \left(\log_{10} e \right) \ln x = A_{\mathrm{T}} \left(1 - \beta_{\mathrm{T}} \ln x \right) = A_{\mathrm{T}} \left(1 - y \right). \tag{E-3}$$

Substituting this into Equation 6-8 yields

$$\frac{1}{S_{\mathrm{CX}}^{\mathrm{typ}}} \sim \left\langle \frac{x}{Q_{\mathrm{CX}}^{\mathrm{str}}} \right\rangle = \left\langle \frac{x}{{A_{\mathrm{T}}}^2 \left(1 - y \right)^2} \right\rangle = \frac{\left\langle x \left(1 - y \right)^{-2} \right\rangle}{{A_{\mathrm{T}}}^2}, \tag{E-4}$$

which is transformed to

$$S_{\mathrm{CX}}^{\mathrm{typ}} \sim {A_{\mathrm{T}}}^2 / F \,, \tag{E-5}$$

where we have defined

$$F \equiv \left\langle x \left(1 - y \right)^{-2} \right\rangle, \tag{E-6}$$

which is obtained in the following.

It is reasonable to assume

$$\left| y \right| = \left| \beta_{\mathrm{T}} \ln x \right| \ll 1 \tag{E-7}$$

because of the following. First, β_{T} is at most approximately 0.05 below 10,000 K:

$$\beta_{\mathrm{T}} = \frac{B_0 \left(\log_{10} e \right)}{A_{\mathrm{T}}} = \frac{0.43429 \times B_0}{A_0 + B_0 \left(4.0646 - \log_{10} T_{\mathrm{r}} \right)} \sim 0.43429 \frac{B_0}{A_0} <\sim 0.05 \,, \tag{E-8}$$

where B_0/A_0 is approximately 1/9 in relevant ionospheric charge-exchange collisions. Second, only $Q_{\mathrm{CX}}(\varepsilon_{\mathrm{r}})$ around x~2 practically contributes to $S_{\mathrm{CX}}(T_{\mathrm{r}})$, as can be predicted from the shape of the integrant in Equation 6-1; thus, ln x is at most approximately 1.

Because of Equation E-7, it is reasonable to take the Taylor expansion as

$$\left(1 - y \right)^{-2} \sim 1 + 2y + 3y^2 + 4y^3 \,. \tag{E-9}$$

Inserting into Equation E-6 yields

$$\begin{aligned} F &\equiv \left\langle x \left(1 - y \right)^{-2} \right\rangle \sim \left\langle x \left(1 + 2y + 3y^2 + 4y^3 \right) \right\rangle \\ &= \left\langle x \right\rangle + 2 \left\langle x \ln x \right\rangle \beta_{\mathrm{T}} + 3 \left\langle x \left(\ln x \right)^2 \right\rangle {\beta_{\mathrm{T}}}^2 + 4 \left\langle x \left(\ln x \right)^3 \right\rangle {\beta_{\mathrm{T}}}^3 \,, \\ &= 1 + C_1 \times \beta_{\mathrm{T}} + C_2 \times {\beta_{\mathrm{T}}}^2 + C_3 \times {\beta_{\mathrm{T}}}^3 \end{aligned} \tag{E-10}$$

where

$$\begin{cases} C_1 \equiv 2 \times \langle x \ln x \rangle = 0.84555 \\ C_2 \equiv 3 \times \left\langle x (\ln x)^2 \right\rangle = 2.4711 \\ C_3 \equiv 4 \times \left\langle x (\ln x)^3 \right\rangle = 2.3699 \end{cases} \quad \text{(E-11)}$$

using Equation C-4.

We derived a typical CXCS for the curve effect in Equation E-5, which is used in Equation 6-7. This typical cross section is called precise type because the corresponding error is within 0.01% in Equation 6-9, as shown in Figure 7g and discussed in Section 7.4.

Acknowledgments

A.I. would like to thank A. P. Hickman for helpful discussions. Physical constants used in the present study are based on the 2018 Committee on Data for Science and Technology (CODATA) recommended values at https://physics.nist.gov/constants and the ninth edition of the international system of units (SI) brochure (2019) at https://www.bipm.org/. We would like to thank Editage (www.editage.com) for English language editing. This work was supported by JSPS KAKENHI Grant 21K03639.

References

Alpher, R. A., & White, D. R. (1959). Optical refractivity of high-temperature gases. 1. Effects resulting from dissociation of diatomic gases. *Physics of Fluids, 2*(2), 153-161. https://doi.org/10.1063/1.1705906

Atkins, P., de Paula, J., & Keeler, J. (2018). *Atkins' physical chemistry* (11th ed.): Oxford University Press.

Banks, P. (1966). Collision frequencies and energy transfer - Ions. *Planetary and Space Science, 14*(11), 1105-1122. https://doi.org/10.1016/0032-0633(66)90025-0

Banks, P. M., & Kockarts, G. (1973). *Aeronomy, Part A*. New York: Academic Press.

Bruno, D., Catalfamo, C., Capitelli, M., Colonna, G., De Pascale, O., Diomede, P., et al. (2010). Transport properties of high-temperature Jupiter atmosphere components. *Physics of Plasmas, 17*(11), 112315. https://doi.org/10.1063/1.3495980

Capitelli, M., Bruno, D., & Laricchiuta, A. (2013). *Fundamental aspects of plasma chemical physics transport*. New York: Springer.

Dalgarno, A. (1958). The mobilities of ions in their parent gases. *Philosophical Transactions of the Royal Society of London. Series A, Mathematical and Physical Sciences, 250*(982), 426-439. https://doi.org/10.1098/rsta.1958.0003

Dalgarno, A., McDowell, M. R. C., & Williams, A. (1958). The mobilities of ions in unlike gases. *Philosophical Transactions of the Royal Society of London. Series A, Mathematical and Physical Sciences, 250*(982), 411-425. https://doi.org/10.1098/rsta.1958.0002

Gioumousis, G., & Stevenson, D. P. (1958). Reactions of gaseous molecule ions with gaseous molecules. 5. Theory. *Journal of Chemical Physics, 29*(2), 294-299. https://www.doi.org/10.1063/1.1744477

Heiche, G., & Mason, E. A. (1970). Ion mobilities with charge exchange. *The Journal of Chemical Physics, 53*(12), 4687-4696. https://doi.org/10.1063/1.1673997

Hickman, A. P., Medikeri-Naphade, M., Chapin, C. D., & Huestis, D. L. (1997a). Fine structure effects in the O^+–O collision frequency. *Geophysical Research Letters, 24*(2), 119-122. https://doi.org/10.1029/96gl03797

Holstein, T. (1952). Mobilities of positive ions in their parent gases. *Journal of Physical Chemistry, 56*(7), 832-836. https://doi.org/10.1021/j150499a004

Ieda, A. (2020). Ion-neutral collision frequencies for calculating ionospheric conductivity. *Journal of Geophysical Research-Space Physics, 125*, e2019JA027128. https://doi.org/10.1029/2019JA027128

Ieda, A. (2021). Atomic oxygen ion-neutral collision frequency models at ionospheric temperatures. *Journal of Geophysical Research-Space Physics, 126*, e2020JA028441. https://doi.org/10.1029/2020JA028441

Ieda, A., Oyama, S., Vanhamäki, H., Fujii, R., Nakamizo, A., Amm, O., et al. (2014). Approximate forms of daytime ionospheric conductance. *Journal of Geophysical Research-Space Physics, 119*(12), 10397-10415. https://doi.org/10.1002/2014ja020665

Kihara, T., Taylor, M. H., & Hirschfelder, J. O. (1960). Transport properties for gases assuming inverse power intermolecular potentials. *Physics of Fluids, 3*(5), 715-720. https://doi.org/10.1063/1.1706115

Knof, H., Mason, E. A., & Vanderslice, J. T. (1964). Interaction energies, charge exchange cross sections, and diffusion cross sections for N^+–N and O^+–O collisions. *The Journal of Chemical Physics, 40*(12), 3548-3553. https://doi.org/10.1063/1.1725050

Langevin, P. (1905). A fundamental formula of kinetic theory. *Annales De Chimie Et De Physique, 5*, 245-288.

Laricchiuta, A., Bruno, D., Capitelli, M., Catalfamo, C., Celiberto, R., Colonna, G., et al. (2009). High temperature Mars atmosphere. Part I: transport cross sections. *European Physical Journal D, 54*(3), 607-612. https://doi.org/10.1140/epjd/e2009-00192-7

Levin, E., & Wright, M. J. (2004). Collision integrals for ion-neutral interactions of nitrogen and oxygen. *Journal of Thermophysics and Heat Transfer, 18*(1), 143-147. https://doi.org/10.2514/1.2552

Mason, E. A., & Vanderslice, J. T. (1959). Mobility of hydrogen ions (H^+,H_2^+,H_3^+) in hydrogen. *Physical Review, 114*(2), 497-502. https://doi.org/10.1103/PhysRev.114.497

McDaniel, E. W. (1989). *Atomic collisions: Electron and photon projectiles*. New York: Wiley.

Murphy, A. B. (1995). Transport-coefficients of air, argon-air, nitrogen-air, and oxygen-air plasmas. *Plasma Chemistry and Plasma Processing, 15*(2), 279-307. https://doi.org/10.1007/bf01459700

Murphy, A. B. (2000). Transport coefficients of hydrogen and argon-hydrogen plasmas. *Plasma Chemistry and Plasma Processing, 20*(3), 279-297. https://doi.org/10.1023/a:1007099926249

Murphy, A. B. (2012). Transport coefficients of plasmas in mixtures of nitrogen and hydrogen. *Chemical Physics, 398*, 64-72. https://doi.org/10.1016/j.chemphys.2011.06.017

Pesnell, W. D., Omidvar, K., & Hoegy, W. R. (1993). Momentum-transfer collision frequency of O^+–O. *Geophysical Research Letters, 20*(13), 1343-1346. https://doi.org/10.1029/93gl01597

Pesnell, W. D., Omidvar, K., Hoegy, W. R., & Wharton, L. E. (1994). O^+–O collision frequency in high-speed flows. *Journal of Geophysical Research, 99*(A11), 21375-21382. https://doi.org/10.1029/94ja01650

Rapp, D., & Francis, W. E. (1962). Charge exchange between gaseous ions and atoms. *Journal of Chemical Physics, 37*(11), 2631-2645. https://doi.org/10.1063/1.1733066

Schunk, R. W., & Nagy, A. F. (2009). *Ionospheres : Physics, plasma physics, and chemistry* (2nd ed.). New York: Cambridge University Press.

Stallcop, J. R., Partridge, H., & Levin, E. (1991). Resonance charge transfer, transport cross sections, and collision integrals for $N^+(^3P)$–$N(^4S^0)$ and $O^+(^4S^0)$–$O(^3P)$ interactions. *The Journal of Chemical Physics, 95*(9), 6429-6439. https://doi.org/10.1063/1.461563

Stebbings, R. F., Smith, A. C. H., & Ehrhardt, H. (1964). Charge transfer between oxygen atoms and O^+ and H^+ ions. *Journal of Geophysical Research, 69*(11), 2349-2355. https://doi.org/10.1029/JZ069i011p02349

Wolf, F. A., & Turner, B. R. (1968). Energy dependence of charge-transfer reactions in thermal and low-electron-volt region. *Journal of Chemical Physics, 48*(9), 4226-4233. https://doi.org/10.1063/1.1669761

Wright, M. J., Hwang, H. H., & Schwenke, D. W. (2007). Recommended collision integrals for transport property computations Part 2: Mars and Venus entries. *Aiaa Journal, 45*(1), 281-288. https:/www.doi.org/10.2514/1.24523